Profiling of a Saharan dust outbreak based on a synergy between active and passive remote sensing

Jean-François Léon,[1] Didier Tanré,[1] Jacques Pelon,[2] Yoram J. Kaufman,[3] Jim M. Haywood,[4] and Bernadette Chatenet[5]

Received 19 July 2002; revised 4 October 2002; accepted 26 November 2002; published 9 September 2003.

[1] Spaceborne lidars will give a new view of the vertical distribution of atmospheric aerosols and clouds. CALIPSO will be launched in the fall of 2004 and will provide, for the first time, a global picture of the profile of atmospheric scattering layers using an onboard lidar radiated at 0.532 and 1.064 μm. CALIPSO will fly in an orbital formation with passive radiometers, such as the Moderate resolution Imaging Spectrometer (MODIS) and the Polarization and Directionality of Earth's Reflectance (POLDER) instruments, that monitor Earth's atmosphere. The purpose of this paper is to analyze the improvement in retrieval capabilities of profiles of aerosol optical properties using a synergy between passive and active (lidar) remote sensing techniques. Aerosol properties derived from the MODIS spectroradiometer are used to constrain the inversion of the lidar signal in terms of aerosol optical thickness and effective radius. We use the lidar spectral backscattering coefficient between 0.532 and 1.064 μm to determine the profile of backscatter-to-extinction ratio. The effective radius of an assumed bimodal aerosol size distribution is then retrieved as a function of the altitude. A sensitivity analysis demonstrates the robustness of the inversion procedure in case of noise detection and calibration error. The algorithm has been tested during the Saharan dust experiment, which took place in the northeastern tropical Atlantic in September 2000. The vertical profile of extinction compares well with in situ measurements of the aerosol extinction. Profiles derived from lidar measurements on 25 September highlight the presence of the Saharan air layer located between 2.2 and 4.5 km with particle effective radii of 1.19 ± 0.6 μm. Another dust layer within the sub-Saharan transition layer over the marine boundary layer is also observed, with particle radii significantly smaller than within the Saharan air layer. *INDEX TERMS:* 0305 Atmospheric Composition and Structure: Aerosols and particles (0345, 4801); 0360 Atmospheric Composition and Structure: Transmission and scattering of radiation; 3360 Meteorology and Atmospheric Dynamics: Remote sensing; *KEYWORDS:* aerosols, lidar, Saharan dust

Citation: Léon, J.-F., D. Tanré, J. Pelon, Y. J. Kaufman, J. M. Haywood, and B. Chatenet, Profiling of a Saharan dust outbreak based on a synergy between active and passive remote sensing, *J. Geophys. Res.*, *108*(D18), 8575, doi:10.1029/2002JD002774, 2003.

1. Introduction

[2] Tropospheric aerosol radiative forcing is a critical component of the global climate. However, the lack of a detailed knowledge on physical, chemical and optical properties results in aerosol being one of the major sources of uncertainty for climate forcing assessments [*Intergovernmental Panel on Climate Change*, 2001]. Recent intensive field campaigns and development of observational networks aim at reducing the uncertainty on aerosol direct and indirect radiative effects. Moreover satellite remote sensing provides a unique observation of aerosols at a global scale. The new generation of satellite sensors, e.g., the Moderate Resolution Imaging Spectrometer (MODIS) [*Salomonson et al.*, 1989] aboard the Terra satellite launched in December 1999, provides well-selected multispectral observations. A specific algorithm has been dedicated to the use of the spectral capacity of MODIS to routinely monitor the spectral aerosol optical thickness and aerosol effective radius over the oceans [*Tanré et al.*, 1997] and the spectral aerosol optical thickness over the land [*Kaufman et al.*, 1997b]. Regarding the vertical distribution of aerosols, the Laser In Space Technology Experiment [*Winker et al.*, 1996] has proven the ability of spaceborne backscattering lidars to perform measurements of the aerosol vertical structure at a high resolution from

[1]Laboratoire d'Optique Atmosphérique, Centre National de le Recherche Scientifique, Université de Lille 1, Lille, France.
[2]Service d'Aéronomie, Centre National de le Recherche Scientifique, Université Pierre et Marie Curie, Paris, France.
[3]Laboratory for Atmospheres, NASA Goddard Space Flight Center, Greenbelt, Maryland, USA.
[4]Meteorological Office, Bracknell, UK.
[5]Laboratoire Inter-Universitaire des Systèmes Atmosphériques, Centre National de le Recherche Scientifique, Université Paris 12, Paris, France.

0148-0227/03/2002JD002774

space. The Cloud-Aerosol Lidar and Infrared Pathfinder Satellite Observation (CALIPSO) [*Winker et al.*, 2002] will be launched in the fall of 2004. The CALIPSO lidar is a frequency-doubled Nd:YAG laser which transmit laser light simultaneously at 0.532 and 1.064 μm and will fly in an orbital formation with other multisensors platforms carrying passive remote sensing instruments dedicated to Earth's system observation. MODIS is also aboard the Aqua satellite launched in May 2002 and that will be flying in formation with CALIPSO. Passive remote sensing instruments [*Kaufman et al.*, 1997a; *King et al.*, 1999] provide a global picture of the aerosol optical thickness distribution; however, they cannot retrieve the vertical dimension which is of importance for aerosol transport and evolution. A synergetic approach using passive and active instruments is then able to significantly enhance our understanding of the aerosol distribution at a global scale.

[3] The evaluation of the aerosol extinction coefficient from the lidar return signal requires to solve the ambiguity between scattering and extinction of the laser beam by aerosol particles. Numerous inversion techniques were proposed for the retrieval of physical particle parameters using single radiated wavelength lidar [*Fernald et al.*, 1972; *Klett*, 1981], spectral lidar [*Müller et al.*, 1999a, 1999b], multiangular measurements [*Sicard et al.*, 2002], or by use of the Raman effect [*Ansmann et al.*, 1990; *Ferrare et al.*, 2000]. Passive observations across the shortwave spectrum strongly increase our ability to solve the ill-posed inverse problem of lidar remote sensing since it allows the evaluation of the size or the refractive index of particles which control the backscatter-to-extinction ratio.

[4] The aim of this paper is to introduce a new method for an optimal use of two wavelength channels of the future spaceborne lidar. For this purpose, we propose to use simultaneous information on aerosol optical properties over ocean derived from the MODIS aboard the Terra satellite and lidar measurements simulating the CALIPSO data. Airborne lidar profiles were acquired simultaneously with the Terra satellite overpass during the Saharan Dust Experiment. The first section gives a description of the basis of the MODIS retrieval and how the MODIS-derived aerosol parameters are merged into the lidar retrieval. The second section is dedicated to the application of the tentative synergy to the field data collected during the Saharan Dust Experiment and the characterization of the vertical profile of a Saharan dust outbreak occurring over the north tropical Atlantic ocean.

2. Material and Method

2.1. MODIS

[5] MODIS has been launched successfully in December 1999 on board NASA's spacecraft Terra and began collecting data in March 2000. The instrument performs spectral measurements from 0.415 to 14.235 μm. The resolution of the subnadir pixel is from 250 m × 250 m to 1 km × 1 km while the aerosol parameters are retrieved at a resolution of 10 × 10 km. An operational algorithm, based on a look-up table approach, has been developed for deriving aerosol properties over dark ocean surface [*Tanré et al.*, 1997]. The algorithm uses 6 spectral channels ranging from 0.55 to 2.13 μm. Top-of-atmosphere leaving radiances are computed for 9 aerosol models (i.e., size distribution and refractive index) and 5 values of the aerosol optical thickness from 0 (Rayleigh atmosphere) to 2. Each of the aerosol size distributions is assumed to be lognormal. Aerosol models are divided into 4 small and 5 large modes, corresponding to the accumulation and coarse mode [*Whitby*, 1978]. The contribution to the scattered light by the particles of the nucleation mode (particles smaller than 0.01 μm) is weak in the spectral range of MODIS and this mode is not considered. Table 1 sums up the physical properties of the aerosol models used in the look-up table. Models numbered from 1 to 4 (median radius from 0.07 to 0.10 μm) belong to small particle mode while models numbered from 5 to 9 (median radius from 0.40 up to 0.80 μm) belong to the large particle mode. The effective radii (defined as the ratio of the third to the second moment of the size distribution) range between 0.1 and 0.24 μm for small mode and 0.97 and 2.36 for large mode.

Table 1. Microphysical and Optical Properties of the MODIS Aerosol Models

Model Number	r_m	σ_m	r_{eff}	σ_{eff}	$m_r - m_i i$	a^*	$\varphi_p(\lambda_1)$	$\varphi_p(\lambda_2)$
1	0.07	1.49	0.10	1.17	1.45−0.0035i	1.72	0.023	0.058
2	0.06	1.82	0.15	1.39	1.45−0.0035i	1.40	0.016	0.026
3	0.08	1.82	0.19	1.39	1.40−0.0020i	1.23	0.013	0.020
4	0.10	1.82	0.24	1.39	1.40−0.0020i	1.18	0.013	0.017
5	0.40	1.82	0.97	1.39	1.45−0.0035i	0.36	0.035	0.025
6	0.60	1.82	1.46	1.39	1.45−0.0035i	−0.03	0.035	0.031
7	0.80	1.82	1.94	1.39	1.45−0.0035i	−0.25	0.033	0.034
8	0.60	1.82	1.46	1.39	1.53−0.0010i	0.13	0.090	0.071
9	0.50	2.22	2.36	1.66	1.53−0.0010i	−0.10	0.073	0.071

[6] According to *Wang and Gordon* [1994], the multiple scattering radiance L_λ from two lognormal modes can be approximated by the weighted average of the radiance for each individual mode for the same optical thickness.

$$L_\lambda = \eta L^s_\lambda(\mu_s, \mu_s, \phi_v) + (1 - \eta) L^l_\lambda(\mu_s, \mu_s, \phi_v) \quad (1)$$

[7] $L^s_\lambda(\mu_s, \mu_s, \phi_v)$ and $L^l_\lambda(\mu_s, \mu_s, \phi_v)$ are the radiances of the small (s) and large (l) mode, respectively. The parameter η is retrieved by minimizing the difference between measured and computed radiances in a least square meaning. Primary aerosol products derived from MODIS include: spectral aerosol optical thickness (AOT), effective radius of the size distribution, and the fraction of the total aerosol optical thickness coming from the fine aerosol mode. MODIS primary aerosol products have been validated using Sun photometer measurements performed in the frame of the Aerosol Robotic Network, AERONET [*Holben et al.*, 1998]. The spectral AOT over oceans is retrieved within an accuracy of $(0.03 \pm 0.05 \times AOT)$ [*Remer et al.*, 2002]. The accuracy falls within the one expected by *Tanré et al.* [1997]. The absolute accuracy on the effective radius is ±0.1 μm. The good agreement found between MODIS and Sun Photometer retrieval points out that both the aerosols models chosen for the inversion and the method are suitable for aerosol monitoring using multispectral data. Caution needs to be taken because MODIS retrievals are selected to correspond to cloud-screened AERONET data. However, we will use this approach to analyze the lidar return signal at

the two wavelengths only in cloud-free areas both observed in the MODIS and lidar data.

2.2. New Lidar Algorithm

2.2.1. Analysis of the Lidar Signal

[8] The optical power $P(\lambda, z)$ backscattered to the telescope by aerosols and molecules located at an altitude z is given by *Zuev and Naats* [1983]:

$$P(\lambda,z) = \frac{C(\lambda)}{(z_a - z)^2}\,\beta(\lambda,z)\,T^2(z,z_a,\lambda), \tag{2}$$

where $C(\lambda)$ is a calibration factor depending on the wavelength λ. $C(\lambda)$ can be determined by matching the upper portion of the backscattering profile to pure molecular scattering. β is the sum of the aerosol and molecular backscattering coefficients. z_a is the altitude of the laser source. $T(z, z_a)$, the layer transmission between z and z_a for a downwarding system is given by:

$$T(z,z_a,\lambda) = \exp\left(-\int_z^{z_a}\{\psi(\lambda,z')\alpha_p(\lambda,z') + \alpha_m(\lambda,z')\}\,dz'\right), \tag{3}$$

where $\alpha_{p,m}$ are the extinction coefficient for particles (p) and molecules (m) respectively.

[9] A factor $\psi(\lambda, z')$ is applied to take into account the effect of multiple scattering. Multiple scattering is an additional source of retrieval uncertainty [*Miller and Stephens*, 1999]. However, for airborne measurements in semitransparent layers, we will consider in the following study that $\psi = 1$.

[10] The backscattering and the extinction coefficients are related linearly by the backscattering to extinction ratio (BER), $\varphi_{p,m}$.

$$\varphi_{p,m}(\lambda,z) = \frac{\beta_{p,m}(\lambda,z)}{\alpha_{p,m}(\lambda,z)} \tag{4}$$

Here $\varphi_{p,m}(\lambda, z)$ is the backscattering phase function for molecules (m) and particles (p) normalized to 4π steradian. For molecular scattering, φ_m is constant and equal to $3/8\pi$. φ_p depends on the aerosol size distribution, refractive index and shape and consequently may vary with altitude. For example, φ_p may vary from 0.035 sr^{-1} to 0.045 sr^{-1} in the marine boundary layer depending on the relative concentration of sea salt and sulfates [*Flamant et al.*, 1998]. In the free troposphere this parameter may vary from 0.015 sr^{-1} for pollution haze such has encountered in the north Indian Ocean [*Léon et al.*, 2001; *Pelon et al.*, 2002] to 0.035 sr^{-1} for dust outbreaks observed over the Mediterranean Sea [*Hamonou et al.*, 1999].

[11] Considering an aerosol model composed of a small and a large mode, $\varphi_p(z, \lambda)$ is a function of the spectral dependency of the backscattering coefficient. We define here a pseudo Angström exponent a^* related to the spectral dependency of the backscattering coefficient between $\lambda_1 = 0.532$ or $\lambda_2 = 1.064$ μm.

$$\frac{\beta(\lambda_1)}{\beta(\lambda_2)} = \left(\frac{\lambda_1}{\lambda_2}\right)^{-a^*} \tag{5}$$

[12] The pseudo Angström exponent is simulated using Mie theory for the 20 (4×5) available combinations of one small and one large mode of the MODIS look-up table and with the relative contribution of the small mode to the total extinction (hereinafter called ζ) varying between 0 (only the large mode) to 1 (only the small mode). The backscattering coefficient is estimated using equation (6).

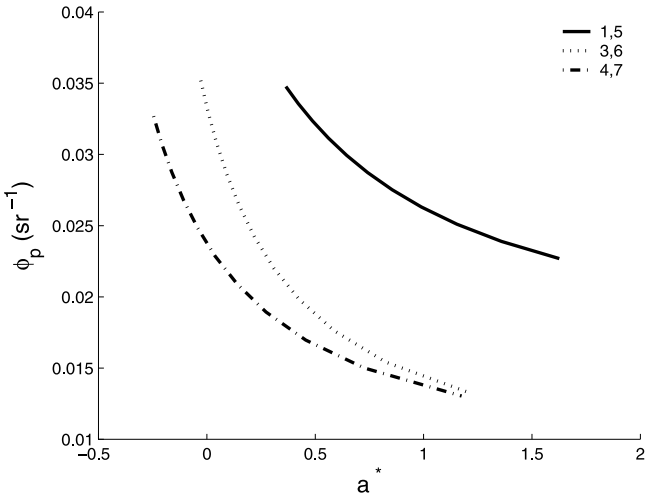

Figure 1. Backscattering-to-extinction ratio at 0.532 μm as a function of the pseudo Ansgström exponent derived from the lidar backscattering coefficient for different mixing of a small and a large mode. Mixing of model 1 and 5 (solid line), model 3 and 6 (dotted line), and model 4 and 7 (dashed line).

$$\begin{cases} \alpha_s(\lambda,z) = \zeta(\lambda,z)\,\alpha_p(\lambda,z) \\ \alpha_l(\lambda,z) = (1-\zeta(\lambda,z))\,\alpha_p(\lambda,z) \\ \beta_p(\lambda,z) = \varphi_p^s(\lambda,z)\,\alpha^s(\lambda,z) + \varphi_p^l(\lambda,z)\,\alpha^l(\lambda,z) \end{cases} \tag{6}$$

[13] Figure 1 presents the variation of $\varphi_p(\lambda_1)$ as a function of a^* for 3 different mixings of a large (in this case sea salt-like particles) and a small (water soluble-like particles) mode. It illustrates the relationship between a^* that is used to derive φ_p from the 2-channel lidar. The solid line corresponds to a mixing of modes 1 and 5, the dotted line to a mixing of modes 3 and 6, and the dashed line to a mixing of modes 4 and 7. Low values of a^* correspond to a major contribution of the large mode while higher values correspond to a major contribution of the small mode. In the case of large particles, the effect of the refractive index may be significant. Indeed, considering model 6 and 8, which have the same effective radius, changing the refractive index from $1.45-0.0035i$ to $1.53-0.0010i$ (see Table 1) increases $\varphi(\lambda_1)$ from 0.035 sr^{-1} to 0.090 sr^{-1} and (λ_2) from 0.031 to 0.071 sr^{-1}.

[14] The absolute accuracy Δa^* depends on the relative accuracy $\delta\beta$ that we can expect in measuring β_p. At the first order, the absolute error Δa^* can be expressed by

$$\Delta a^* = \left(\delta\beta(\lambda_1)^2 + \delta\beta(\lambda_1)^2\right)^{1/2} / \ln(\lambda_2/\lambda_1). \tag{7}$$

[15] Assuming a relative accuracy of 5% in β, then a^* can be measured within 0.1. This precision impacts the evalu-

ation of the backscattering to extinction function and the effective radius. On the basis of Figure 1, the accuracy in φ_p is decreasing when a^* is decreasing for a given backscattering error. The decrease in a^* is due to the increase in the contribution of the large mode of particles to the backscattering coefficient. When considering aerosols that are only in the accumulation mode, φ_p is retrieved within 5 to 10% while for large particles only the accuracy is between 25 and 30%. Owing to this uncertainty and because the aerosol models may not be fully representative of the actual conditions, the measured value of a^* can be out of the bounds of the simulation for a given combination. It results in unphysical solutions where the ζ coefficient is < 0 or > 1. As reported in Table 1, the maximum value of a^* is 1.72 which corresponds to aerosol model 1 when the minimum value of a^* is -0.25 and corresponds to model 7. When the measured wavelength exponent is out of these extreme values, the retrieval of φ_p is not possible. In this case, we adopt the respective upper or lower bounding value of the relationship between φ_p and a^*.

2.2.2. Use of the MODIS Data

[16] The aerosol optical thickness observed by MODIS, $\tau^{MODIS}(\lambda)$ is related to the extinction coefficient α_p derived from lidar measurements by

$$\tau^{MODIS}(\lambda) = \sum_{j=1}^{N} \alpha_p(j,\lambda)\Delta z, \tag{8}$$

where Δz is the lidar vertical resolution dividing the atmosphere into N homogeneous layers starting with level 1 close to the ground. Since the MODIS aerosol optical thickness is not derived at 1.064 μm, it is interpolated from 0.87 and 1.24 μm according to the Angström law. At a given level i, the aerosol transmission $T_p(i, \lambda)$ is given by

$$T_p(i,\lambda) = \exp\left\{-\tau^{MODIS}(\lambda) + \sum_{j=1}^{i-1}\alpha_p(j,\lambda)\Delta z\right\}. \tag{9}$$

For the *ith* layer, $\beta_p(i, \lambda)$ can be obtained from equation (2) at wavelength λ_1 and λ_2, then $a^*(i)$ further is obtained from equation (5). $\zeta(i, \lambda)$, the relative contribution of the small mode to the total extinction is then derived by interpolating into a look-up table built for each of the 20 possible combinations. Owing to the one-to-one relationship between the pseudo Angström a^* and the relative contribution ζ for a given set a small and a large mode, the derived BER, φ_p is unique. α_j, the extinction coefficient is then estimated using equation (4). The procedure is applied to next layer j until reaching the top of the atmosphere. The introduction of τ^{MODIS} in the two-way transmission term restrains the propagation of overestimation or underestimation of α_j from the lower layers to the upper layers; the vertical integration of the aerosol extinction coefficient derived from the lidar should give an AOT equal to the one derived from MODIS.

[17] However, several combinations of a small and a large mode can lead to an AOT close to the MODIS value. To better constrain the retrieval and select the best set of aerosol models, we introduce a criteria on the effective radius. The effective radius is the driving size parameter regarding the optical properties of particles in the solar reflected radiances [*Tanré et al.*, 1996]. The effective radius of the layer is evaluated using the retrieved ζ value following

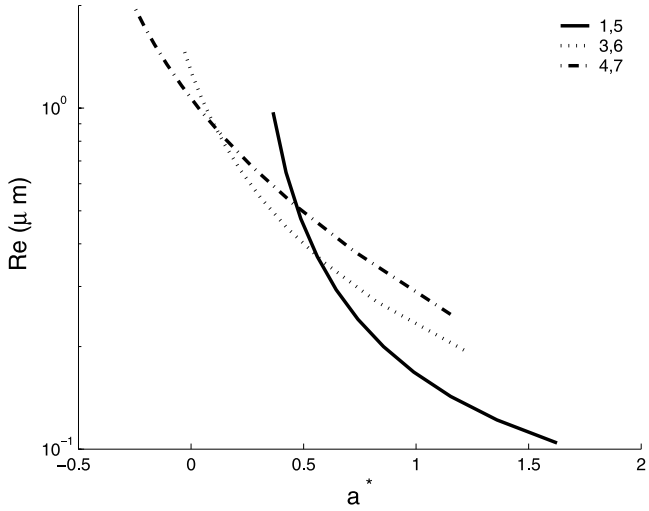

Figure 2. Same legend as Figure 1 but for the effective radius.

$$r_{eff}(z) = \frac{\zeta(z)M_s^3/\kappa_s + (1-\zeta(z))M_l^3/\kappa_l}{\zeta(z)M_s^2/\kappa_s + (1-\zeta(z))M_l^2/\kappa_l} \tag{10}$$

with

$$M_{s,l}^i = \int_0^\infty r^i n_{s,l}(r)dr, \tag{11}$$

where $\kappa_{s,l}$, $n_{s,l}(r)$ are the extinction cross section and particle normalized size distribution for the small and the large mode, respectively; r is the particle radius. Figure 2 illustrates the variation of the effective radius as a function of a^* for the same set of models as in Figure 1. The columnar averaged effective radius, $\langle R_{eff}^{lidar}\rangle$, is computed from equation (10). The total AOT and columnar averaged effective radius is so computed for each of the 20 profiles. Owing to the respective uncertainties in the AOT and the effective radius, we have to consider the total range of possible solutions, and we retain only the set of profiles for which both the total AOT and the columnar averaged effective radius fall within the accuracy of the retrieval of this parameter by the MODIS. On the basis of the uncertainty in the MODIS-retrieved aerosol parameters given in section 2.1, the criteria to select the best lidar retrievals are then:

$$\begin{cases} |AOT_{\lambda_1,\lambda_2}^{lidar}| \le AOT_{\lambda_1,\lambda_2}^{MODIS} \pm 0.05 \times AOT_{\lambda_1,\lambda_2}^{MODIS} \pm 0.03 \\ |\langle R_{eff}^{lidar}\rangle| \le R_{eff}^{MODIS} \pm 0.1\mu m \end{cases} \tag{12}$$

3. Results

3.1. Application to Field Experiment

[18] The Saharan Dust experiment (SHADE) was designed to characterize African dust transport over the

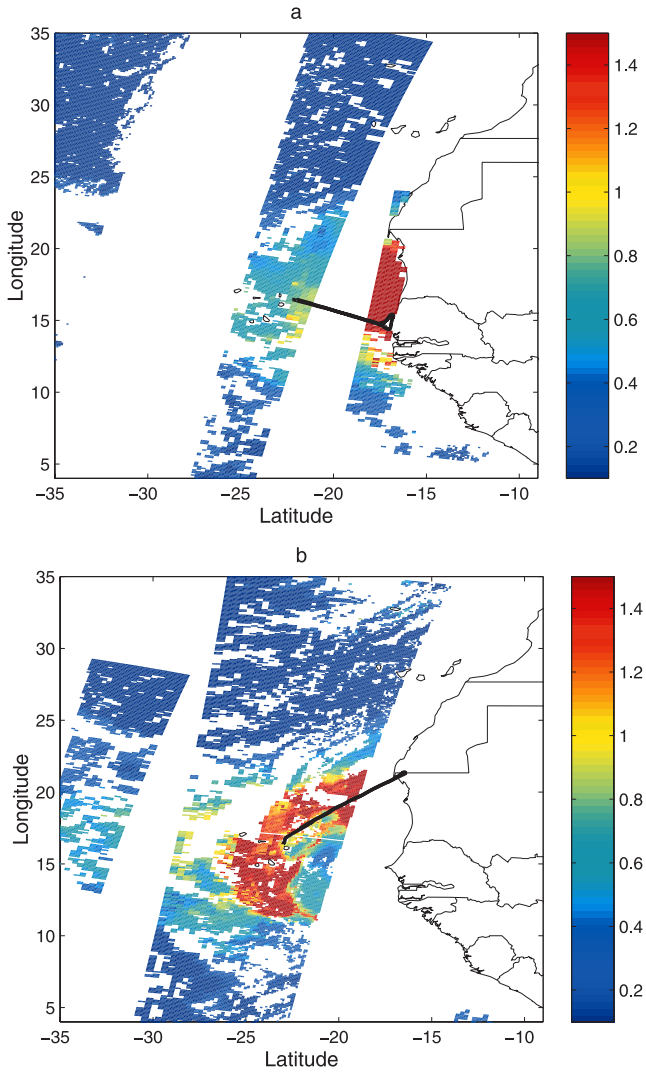

Figure 3. MODIS aerosol optical thickness at 550 nm on (a) 25 September and (b) 26 September 2000.

northeastern tropical Atlantic, A set of observations similar to the data that will be acquired by the Aqua-Train was made available [*Tanré et al.*, 2003] and used to test the proposed method. Observations were acquired between the west African coast and the Cape Verde archipelago located 500 km west of the African coast. This location is well-known to be the main area of dust transport over the tropical Atlantic [*Chiapello et al.*, 1997]. Combined ground-based, airborne and satellite observations were performed from 21 to 29 September 2000. The ground-based station of Sal Island (16.43°N, 22.56°W) and Dakar (14.38°N, 16.95°W) were equipped with an automatic Cimel Sun photometer of the Aerosol Robotic Network (AERONET) [*Holben et al.*, 1998]. Sun and the sky spectral radiance at four wavelengths (0.44, 0.67, 0.87, and 1.02 μm) were measured. The AERONET inversion algorithm [*Dubovik and King*, 2000], provides the spectral aerosol complex refractive index and the size distribution ($0.05 \leq r \leq 15$ μm). Measurements of the vertical distribution of scattering layers were performed using the backscattering lidar LEANDRE-1 [*Pelon et al.*, 1990] on board the French research aircraft Mystere-20 (M-20). The laser is a Nd:Yag delivering 10 *ns* pulses of 40 and 190 *mJ* in the 0.532 and 1.064 μm channel respectively at a frequency of 12 *Hz*. Considering the average speed of the aircraft, the resulting horizontal and vertical resolution is about 15 m. Dual polarization is also performed at 0.532 μm. On 25 September 2000, in situ measurements of the aerosol scattering and extinction coefficients were performed on board the U.K. C-130 research aircraft. The C-130 was equipped with the standard instrumentation detailed in the work of *Haywood et al.* [2003]. Particulate absorption of radiation at wavelength 0.567 μm was measured with a Radiance Research Particle Soot Absorption Photometer (PSAP). Aerosol scattering was determined at 3 wavelengths (0.45, 0.55, 0.70 μm) with a TSI 3563 nephelometer. Corrections were applied to the data from the PSAP to account for inaccuracies in the flow rate, area of exposure of the filter, and absorption artifacts following the analysis of *Bond et al.* [1999]. Corrections to the nephelometer were applied following the results of *Anderson and Ogren* [1998] to consider the truncation of forward scattered radiation.

3.2. Overview of the Observations

[19] On 25 and 26 September a transport of dust is observed over the area of interest. The minimum and maximum aerosol optical thicknesses retrieved by the Dakar Sun photometer are 0.85 and 1.5 on 25 September and respectively 0.28 and 0.80 on 26 September. Minimum and maximum AOT observed at Sal Island are 0.32 and 0.57 on 25 September, and 0.60 and 1.70 on 26 September. Figures 3a and 3b show the aerosol optical thickness derived from MODIS on 25 and 26 September, respectively. The areas where the retrieval is not possible, like cloudy sky, land surface or specular reflectance zone, are in white. The black solid lines plotted between the western African coast and the Cape Verde Islands are the ground tracks of the Mystere-20 research aircraft acquisition. Acquisition time of MODIS data is around 13 UT. The observed situation corresponds to the advection of a heavy dust plume from the west coast of Mauritania moving to the Cape Verde archipelago.

[20] Figures 4a and 4b present the attenuated lidar backscattering coefficient measured on 25 and 26 September as a function of the longitude. Lidar signal is range-corrected and normalized to molecular scattering. The lidar attenuated backscattering coefficient corresponds to the product of the total atmospheric backscattering coefficient (particles and molecules) by the two-way transmission. On both days, lidar cross sections reveal the presence of a dust layer above the marine boundary layer and up to 5 km high.

[21] On 26 September, the main feature of the vertical structure of atmosphere is the presence of a deep dust layer (about 1 km thickness) between 2 and 3 km high. A second layer is observed above 3 km up to 5–6 km with low raw backscatter coefficient compared to the lower layer. Many cirrus just below the flight level of the aircraft are observed during the flight. Decreases in the 2-D attenuated backscattering coefficient in Figure 4b are due to the attenuation by cirrus clouds. No dropsondes are available on 26 September because the C-130 was grounded for technical reasons.

[22] On 25 September, two layers can be observed over the marine boundary layer, the upper one located between 2 and 5 km, and the lower one at about 1 km high. Increase in

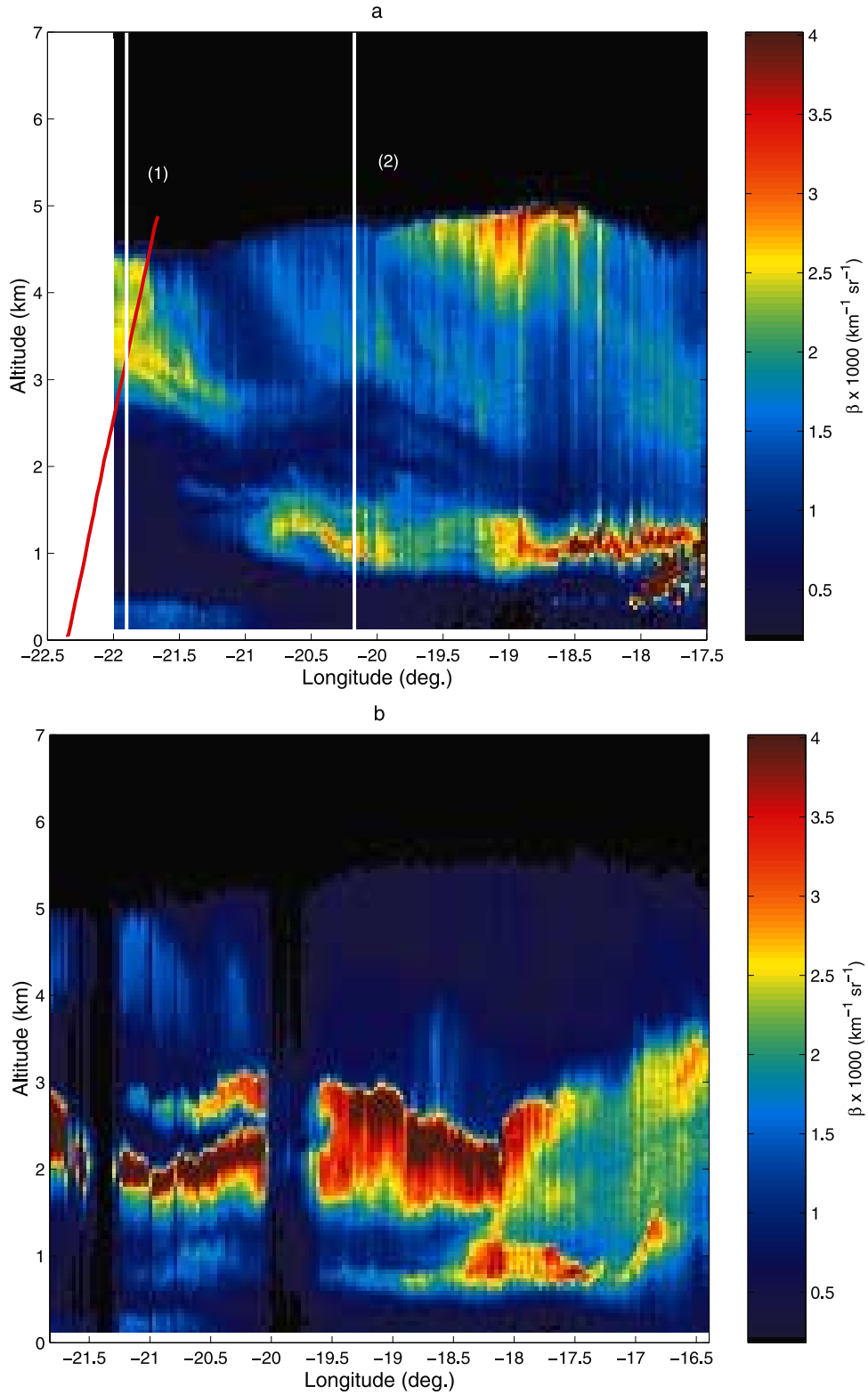

Figure 4. Lidar attenuated backscattering coefficients measured below the track of the air plane on (a) 25 September and (b) 26 September 2000. The red line on the upper panel corresponds to the C-130 track. The two white lines number (1) and (2) represent the lidar profile plotted in Figure 6.

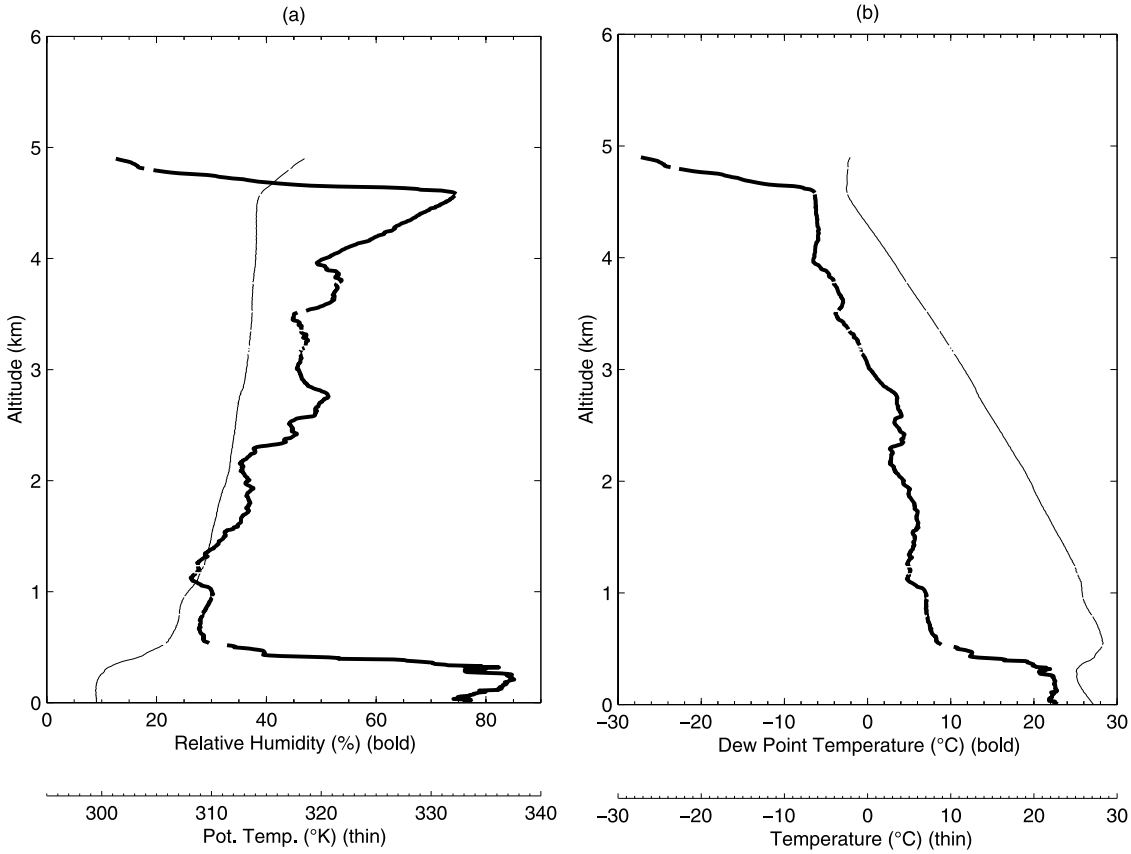

Figure 5. (a) Vertical profile of (bold line) the relative humidity, and (thin line) the potential temperature. (b) Vertical profile of (bold line) dew point temperature and (thin line) temperature measured by means of a dropsonde dropped close to the Sal Island.

the attenuated backscattering coefficient can be observed at about $-20°$ longitude due to water condensation.

[23] The vertical profile of meteorological parameters have been measured thanks to dropsondes launched from the C-130 research aircraft. Figures 5a and 5b show the vertical profiles of temperature, dew point temperature, potential temperature, and the relative humidity, measured by dropsonde at $-20.43°$ in longitude. The uppermost layer (so-called the Saharan air layer [*Prospero and Carlson*, 1972]) is limited by a strong inversion in the potential temperature at the top. This inversion is associated with an increase in the relative humidity up to 80%. A second layer (the sub-Saharan transition layer [*Karyampudi et al.*, 1999]) also observed in Figure 4a is located above the marine boundary layer in an area dryer than the aloft layer.

3.3. Comparison of Lidar Retrieval With in Situ Data

[24] We analyze now the profiles measured near the Sal Island on 25 September 2000. The Terra/MODIS performed observations over the field area around 13:00 UT and airborne measurements were performed within 3 hours after the satellite overpass. The advection of the dust plume between the satellite overpass and the airborne lidar acquisition is considered by using the wind speed and direction measured by meteorological dropsondes launched from the C-130. At 3 km high, the wind speed is 12 ms^{-1} and the wind direction is 120°. All the lidar shots inside a same MODIS pixel are averaged together.

[25] Figure 6 presents both profiles of the aerosol extinction coefficient measured in situ by the C-130 and retrieved by the lidar on 25 September. The shaded area corresponds to the in situ extinction coefficient measured during the ascent of the C-130 taking into account the measurement errors. The corresponding flight track is plotted (red line) on Figure 4a as a function of altitude and longitude. Two lidar inversions are presented in Figure 6. The positions of lidar profile (1) and (2) are displayed in Figure 4a as white lines. C-130 did not perform measurements exactly in the same area as shown in Figure 4a, red line. Profile (1) is the closest to the in situ measurements. However, it should be noted there is 1 hour difference between the two acquisitions. A very good agreement is found between profile (1) and in situ data between 700 m and 3 km. Profile (2) gives the magnitude of the spatial variability of the dust plume. A second dust layer above the marine boundary layer (MBL) is observed in profile (2) (see also Figure 4a) corresponding to an increase in the extinction coefficient by about a factor 10 compared to profile (1). Unexpected high backscattering coefficient is observed within the MBL between $-22°$ and $-21°$ longitude in Figure 4a, leading to an extinction coefficient which is about twice higher for profile (1) than for profile (2).

[26] Significant differences are observed between in situ and lidar retrievals within the MBL and the upper part of the dust layer. At the upper part of the dust layer, the discrepancy can be explained by the presence of large particles not

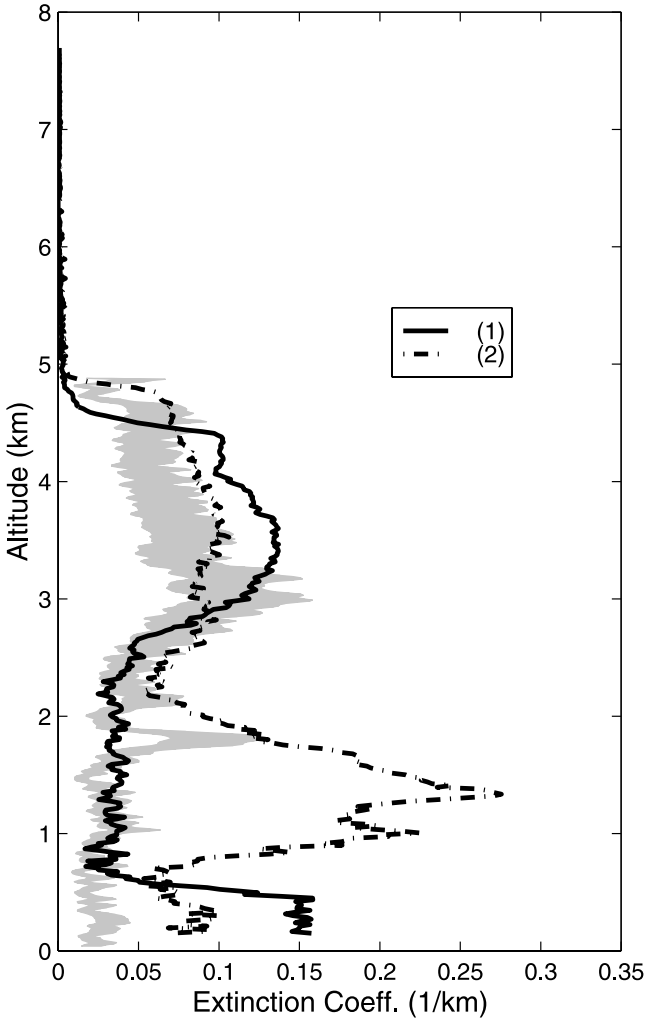

Figure 6. Comparison between (shaded area) in situ measured extinction coefficient obtained from C-130 and (solid and dashed line) lidar-retrieved extinction coefficient on 25 September close for locations (1) and (2).

measured at the top of the dust layer. *Haywood et al.* [2003] suggest a cutoff radius of between 1.3 and 1.7 μm for the Rosemount inlet aboard C-130 resulting in an underestimation of the extinction coefficient within the dust layer. The gap in aerosol extinction between both profiles below 700 m can be explained by the drying of the particles when they are collected inside the onboard nephelometer. Indeed, the relative humidity inside the nephelometer is 50% while it is about 80% inside the MBL. Increasing relative humidity increases the scattering of particles. On the basis of the model of *Kasten* [1969] giving the increase of the scattering coefficient as a function of the relative humidity and *Hegg et al.* [1996] parameter for clean marine air, the nephelometer humidity corrected aerosol extinction would be twice, i.e., 0.06 km^{-1}. It is in a good agreement with the extinction in the MBL retrieved from profile (2), i.e., 0.07 km^{-1}.

3.4. Error Balance

[27] Main sources of error in the retrieval come from (1) signal detection, (2) uncertainty in the calibration and, (3) relevancy of the aerosol models stored in the look-up table. Regarding the third point, nonsphericity of dust particles can significantly affect the value of the backscatter to extinction ratio and the possible presence of two coarse modes of dust and sea salt inside the marine boundary layer cannot be considered in our study. Errors related to signal detection (point 1) and calibration (point 2) affect the backscattering coefficient in both channels. It results in an inaccuracy in the determination of the pseudo Angström exponent and in turn in the evaluation of the backscatter to extinction ratio and the extinction coefficient.

[28] The accuracy of the retrieval is assessed by means of a Monte Carlo simulation. The profile obtained during the Saharan Dust Experiment is used as the undisturbed profile. Calibration and signal detection error expected for the CALIPSO lidar are introduced as a Gaussian noise into the retrieval procedure. The Monte Carlo procedure generates 1000 profiles to reach a Gaussian representation of the process. For each of the 20 combinations, we estimated the columnar optical thickness and effective radius.

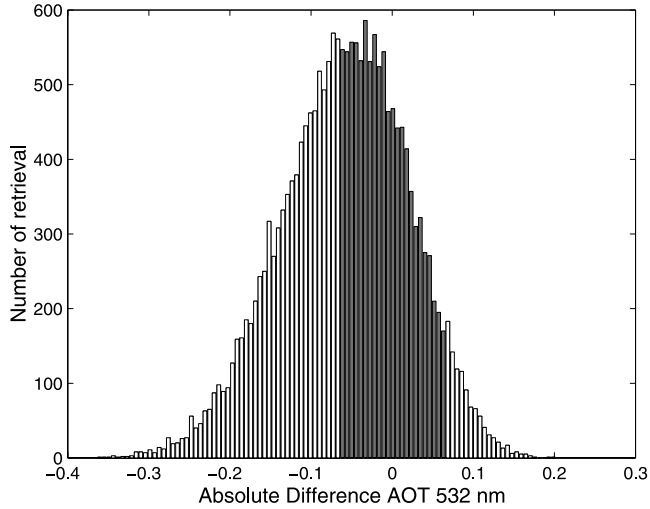

Figure 7. Histogram of the absolute error made on the retrieval of the aerosol optical thickness at 532 nm for all the combinations and all the simulations (20000 cases). Shaded area indicates solutions within the MODIS uncertainty.

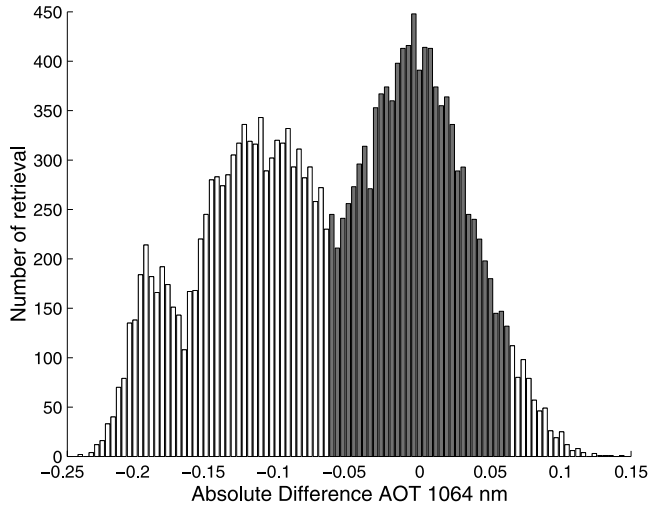

Figure 8. Same as Figure 7 but for the aerosol optical thickness at 1064 nm.

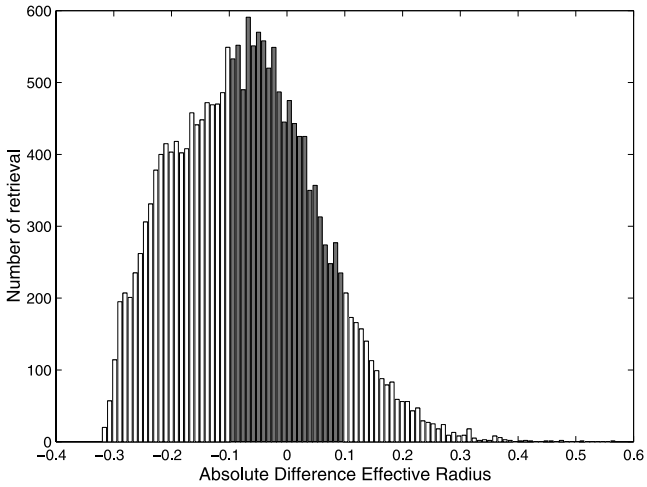

Figure 9. Same as Figure 7 but for the aerosol effective radius.

[29] Figures 7, 8, and 9 are histograms of all the 20000 solutions for the retrieved optical thicknesses at 0.532 μm, at 1.064 μm, and the for columnar effective radius. The relative calibration and signal detection error is 10%. The input value have been subtracted to the solution, so the histograms show how the different retrievals are far from the true solution. Without applying the criteria given in equation (12), the inversion procedure is very robust. The relative error on the aerosol optical thickness at 0.532 μm is 11%, and 24% at 1.064 μm. It is 32% for the columnar averaged effective radius. Increasing uncertainty did not affect significantly the spread of the histograms. However, it introduces a significant bias in the retrieval. This bias is due to unphysical solutions when the ζ coefficient is >1 or <0. Doubling the noise in the data results in a bias that is twice in the retrieval.

[30] The criteria given in equation (12) are a strong constrain in the retrieval because the accuracy in columnar lidar-derived quantities (aerosol optical thickness and average effective radius) are the same as the MODIS-retrieved quantities. Incoherent solutions are rejected (see also shaded areas on Figures 7, 8, and 9). It results that the number of solutions decreases with increasing noise. Applying the criteria, the profile of extinction is retrieved with a relative accuracy of 20% at 1064 μm and 25% at 0.532 μm for a relative calibration and signal detection error of 10%. In this case, we can expect an accuracy of 20% in $\varphi_p(\lambda_1)$ and 15% $\varphi_p(\lambda_2)$. The profile of effective radius is retrieved with an accuracy of 40 to 50% depending on the concentration of large particles.

3.5. Synthesis of the Observations

[31] We present in the following figures the averaged profiles between −23° and −21° longitude. The vertical profile of extinction (Figures 10a and 10b) confirms the presence of the 2-layer structure of the dust in the atmosphere. The altitude of the layers as well as the derived optical parameters are reported in Table 2. The upper dust layer between 2.2 and 4.5 km represents 49% of the AOT at λ_1 and 33% at λ_2. Figure 11 displays φ_p as a function of the altitude for λ_1 and λ_2. φ_p is constant within each aerosol layer, and differs from one layer to the other. φ_p is significantly lower within the lower dust layer and within

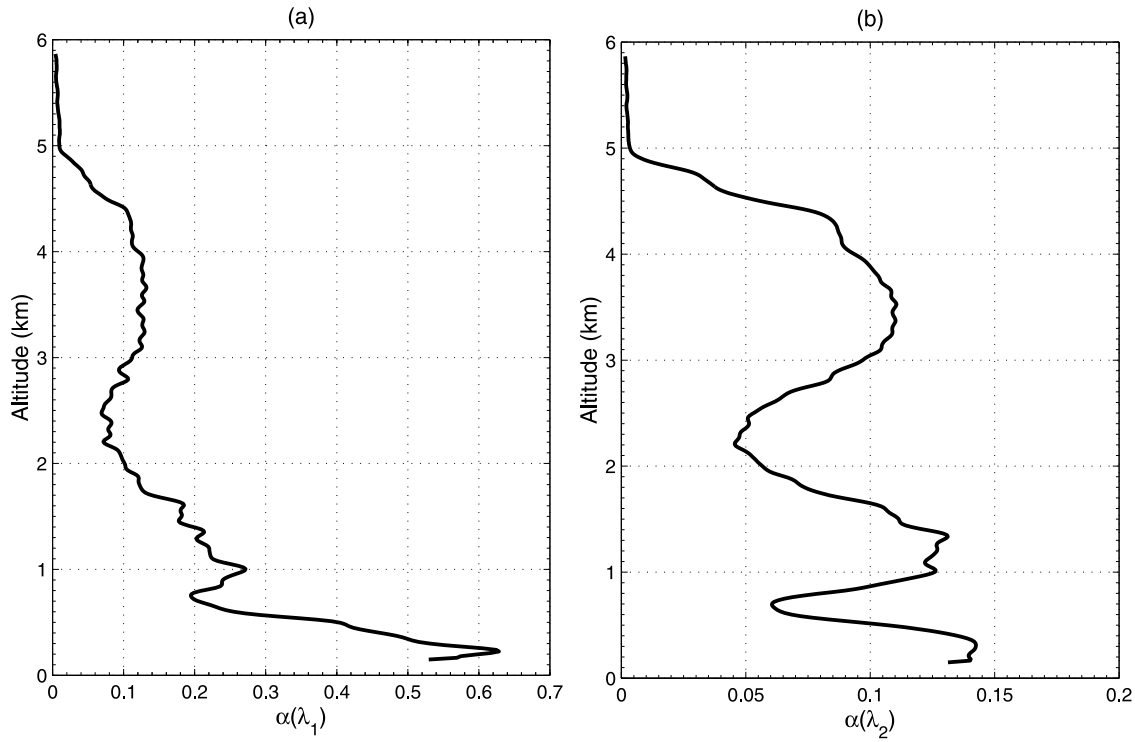

Figure 10. Same as Figure 7 but for the aerosol extinction coefficient at (a) 0.532 μm and (b) 1.064 μm.

Table 2. Optical Properties of the Dust Layers

	Altitude, km	$\tau(\lambda_1)$	$\tau(\lambda_2)$	$\varphi(\lambda_1)$	$\varphi(\lambda_2)$	*Reff*
Marine boundary layer	0.0–0.7	0.24	0.06	0.013	0.018	0.26
Lower dust layer	0.7–2.2	0.26	0.14	0.018	0.026	0.67
Upper dust layer	2.2–4.5	0.25	0.20	0.024	0.031	1.19

the MBL (see Table 2). Within the upper dust layer, φ_p is constant and equal to 0.024 (±0.007) sr^{-1} and $\varphi_p(\lambda_2)$ = 0.031 (±0.005) sr^{-1}. During a Saharan dust episode over the Canary Islands, *Welton et al.* [2000] have derived $\varphi_p(\lambda_1)$ = 0.027 (±0.007) sr^{-1} from micropulse lidar measurements, which is in a good agreement with our retrieval. One should note that this value is significantly lower than $\varphi_p(\lambda_1)$ = 0.035 sr^{-1} obtained using previously reported dust characteristics [*Shettle*, 1984; *Moulin et al.*, 1997] and the Mie theory. φ_p within the MBL is lower than the one expected by *Flamant et al.* [1998] in purely marine conditions but close to what have been observed when the marine atmospheric boundary layer is contaminated with upper level aerosols as observed during INDOEX [*Pelon et al.*, 2002].

[32] The difference in φ_p between the upper and the lower dust layers is associated with a significant difference in the effective radius (Figure 12). Between 2.2 and 4.5 km, the effective radius is 1.19 (±0.6) μm, while it is 0.67 (±0.25) μm within the layer observed over the marine boundary layer. The origin of the aerosol and the aging processes occurring during the transport may explain the difference. The nonsphericity of particles may has also an effect on optical properties. Indeed, using the Mie theory when particles are supposed to be nonspherical can introduce a significant decrease in the expected backscattering to extinction ratio [*Kaufman et al.*, 2003]. It results in turn in an underestimation of the effective radius of nonspherical dust particles.

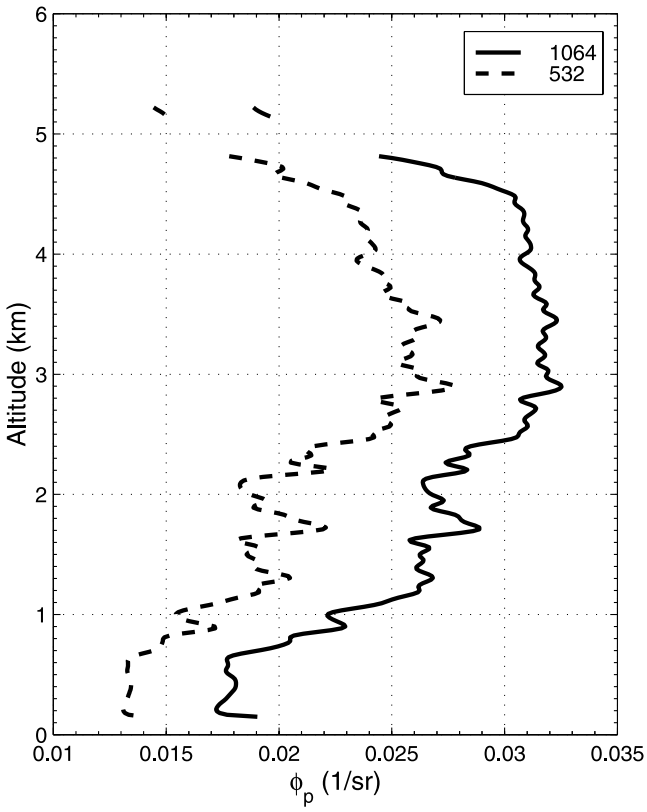

Figure 11. Backscattering to extinction ratio averaged over the profiles acquired between −23° and −21° longitude at (dashed line) 0.532 μm and (solid line) 1.064 μm as a function of the altitude.

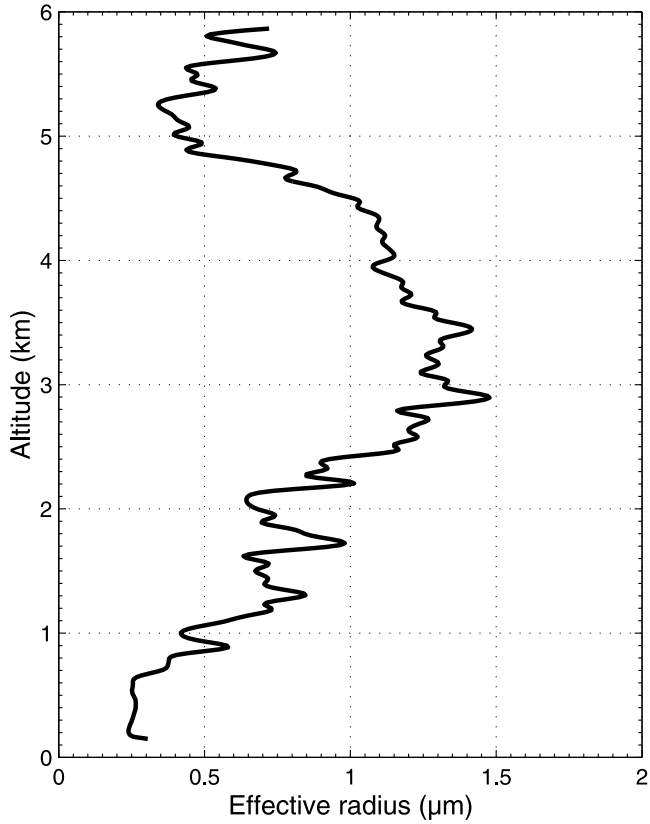

Figure 12. Same caption as for Figure 11 but for the effective radius.

4. Conclusion

[33] Lidar measurements of the aerosol vertical structure are entering a new era thanks to upcoming spaceborne missions carrying backscattering lidars. Deriving the profile of aerosol extinction strongly depends on our ability to prescribe an accurate profile of the backscattering to extinction ratio. Owing to the high spatial and temporal variability of this parameter at the global scale, additional information are required to better constrain the lidar signal inversion. Simultaneous passive spaceborne radiometer measurements can help to reduce the uncertainty remaining on the choice of the backscattering-to-extinction ratio. This paper introduces a new method for a synergetic analysis combining active and passive measurements.

[34] New developments are proposed in order to merge spaceborne lidar and radiometer data. The use of a 2-wavelength lidar radiated at 0.532 and 1.064 μm is optimized by implementing a look-up table approach. The look-up table is based on the aerosol models used in the inversion of the MODIS radiances and assuming a bimodal lognormal aerosol size distribution. The ratio between lidar backscattering coefficients at 0.532 and 1.064 μm is inverted to determine

the relative contribution of the small mode of particles and in return the backscatter-to-extinction ratio for a given layer.

[35] Applied to observations performed during the Saharan Dust Experiment in September 2000 over the northeastern Atlantic ocean. The method reveals the complex structure of the dust transport in the northeastern tropical Atlantic in terms of the vertical distribution and optical and microphysical properties. Vertical profiles show a 2-layer structure of the dust plume with significant different backscattering to extinction ratio between the two layers. $\varphi(532\ nm) = 0.024\ sr^{-1} \pm 0.007\ sr^{-1}$ within the SAL and $0.018\ sr^{-1} \pm 0.004\ sr^{-1}$ within the sub-Saharan layer. We have derived an average effective radius of 1.19 (±0.6) μm for the SAL and 0.67 (±0.25) μm for the sub-Saharan layer. This difference may be due to a different origin of the dust layers, the mixing process of the sub-Saharan layer with the marine boundary layer influenced by natural or anthropogenic submicron particles, or the effect of the nonsphericity of dust particles.

[36] The results obtained from the synergetic algorithm combining active and passive measurements are encouraging. It is shown that the retrieval of aerosol properties can be further improved by the combination of CALIPSO and MODIS. Such a synergy is only possible over cloud-free areas and over ocean surfaces but should work very well for any kind of aerosols. If further developments are required in order to apply this synergy to aerosol remote sensing over land, it can be easily adapted for upwarding lidar systems performing simultaneous observations with a Sun photometer from the ground. Applying the proposed method to CALIPSO lidar will need specific requirements. Indeed, to match the accuracy that we have used in our sensitivity study, CALIPSO profiles need to be horizontally averaged over 25 km for a vertical resolution of 1 km. In these conditions, the MODIS-derived aerosol properties should be reduced to match the resolution of the CALIPSO lidar. The variability of MODIS aerosol optical thickness and size parameter observed along the track of the lidar will then provide valuable additional information in the interpretation of the resultant averaged profiles. The production of such level 4 data involving lidar with other measurements is one of the challenge of the forthcoming space missions.

[37] **Acknowledgments.** This research was funded by Centre National d'Etudes Spatiales. Authors thank Patrick Chazette for helpful discussions. The crew and support staff of the M20 and the Met Office MRF are thanked for their efforts to make the experiment successful.

References

Anderson, T. L., and J. A. Ogren, Determining aerosol radiative properties using the TSI 3563 integrating nephelometer, *Aerosol Sci. Technol.*, *29*, 57–69, 1998.

Ansmann, A., M. Riesbesell, and C. Weitkamp, Measurement of atmospheric extinction profiles with Raman lidar, *Opt. Lett.*, *15*, 746–748, 1990.

Bond, T. C., T. L. Anderson, and D. Campbell, Calibration and intercomparison of filter-based measurements of visible light absorption by aerosols, *Aerosol Sci. Technol.*, *30*, 582–600, 1999.

Chiapello, I., G. Bergametti, B. Chatenet, P. Bousquet, F. Dulac, and E. Santos Soares, Origins of African dust transported over the northeastern tropical Atlantic, *J. Geophys. Res.*, *102*, 13,701–13,709, 1997.

Dubovik, O., and M. D. King, A flexible inversion algorithm for retrieval of aerosol optical properties from Sun and sky radiance measurements, *J. Geophys. Res.*, *105*, 20,673–20,696, 2000.

Fernald, G. F., B. M. Herman, and J. A. Reagan, Determination of aerosol height distributions by lidar, *J. Appl. Meteorol.*, *11*, 482–499, 1972.

Ferrare, R., et al., Comparison of LASE, aircraft, and satellite measurements of aerosol optical properties and water vapor during TARFOX, *J. Geophys. Res.*, *105*, 9935–9947, 2000.

Flamant, C., V. Trouillet, P. Chazette, and J. Pelon, Wind speed dependence of atmospheric boundary layer optical properties and ocean surface reflectance as observed by airborne backscatter lidar, *J. Geophys. Res.*, *103*, 25,137–25,158, 1998.

Hamonou, E., P. Chazette, A. Papayanis, D. Balis, F. Marenco, V. Santacesaria, and G. Ancellet, Characterization of the vertical structure of Saharan dust export to the Mediterranean bassin, *J. Geophys. Res.*, *104*, 22,257–22,270, 1999.

Haywood J. M., et al., Radiative properties and direct radiative effect of Saharan dust measured by the C-130 aircraft during Saharan Dust Experiment (SHADE): 1. Solar spectrum, *J. Geophys. Res.*, *108*(D18), 8577, doi:10.1029/2002JD002687, 2003.

Hegg, A. D., D. S. Covert, M. J. Rood, and P. V. Hobbs, Measurements of aerosol optical properties in marine air, *J. Geophys. Res.*, *101*, 12,893–12,903, 1996.

Holben, N. B., et al., AERONET—A federated instrument network and data archive for aerosol characterisation, *Remote Sens. Environ.*, *66*, 1–16, 1998.

Intergovernmental Panel on Climate Change, *Contribution of Working Group I to the Third Assessment Report of the Intergovernmental Panel on Climate Change*, edited by J. T. Houghton et al., Cambridge Univ. Press, New York, 2001.

Karyampudi, V. M., et al., Validation of the Saharan dust plume conceptual model using Lidar, Meteosat, and ECMWF data, *Bull. Am. Meteorol. Soc.*, *80*, 1045–1075, 1999.

Kasten, F., Visibility in the phase of pre-condensation, *Tellus*, *21*, 631–635, 1969.

Kaufman, Y. J., D. Tanré, H. R. Gordon, T. Nakajima, J. Lenoble, R. Frouin, H. Grassl, B. M. Herman, M. D. King, and P. M. Teillet, Passive remote sensing of tropospheric aerosol and atmospheric correction for the aerosol effect, *J. Geophys. Res.*, *102*, 16,815–16,830, 1997a.

Kaufman, Y. J., D. Tanré, L. A. Remer, E. F. Vermote, A. Chu, and B. N. Holben, Operational remote sensing of tropospheric aerosol over land from EOS moderate resolution imaging spectrometer, *J. Geophys. Res.*, *102*, 17,051–17,067, 1997b.

Kaufman, Y. J., D. Tanré, J.-F. Léon, and J. Pelon, Retrieval of profiles of fine and coarse aerosols using lidar and radiometric space measurements, *IEEE Trans. Geosci. Remote Sens.*, in press, 2003.

King, M. D., Y. J. Kaufman, D. Tanré, and T. Nakajima, Remote sensing of tropospheric aerosols from space: Past present and future, *Bull. Am. Meteorol. Soc.*, *80*, 2229–2259, 1999.

Klett, J. D., Stable analytical inversion solution for processing lidar return signal, *Appl. Opt.*, *20*, 211–220, 1981.

Léon, J.-F., et al., Large-scale advection of continental aerosols during INDOEX, *J. Geophys. Res.*, *106*, 28,427–28,440, 2001.

Miller, S., and G. Stephens, Multiple scattering effects in the lidar pulse stretching problem, *J. Geophys. Res.*, *104*, 22,205–22,219, 1999.

Moulin, C., F. Dulac, C. E. Lambert, P. Chazette, I. Jankowiak, B. Chatenet, and F. Lavenu, Long-term daily monitoring of Saharan dust load over ocean using ISCCP-B2 data: 2. Accuracy of the method and validation using Sun photometer measurements, *J. Geophys. Res.*, *102*, 16,959–16,969, 1997.

Müller, D., U. Wandinger, and A. Ansmann, Microphysical particle parameters from extinction and backscatter lidar data by inversion with regularization: Theory, *Appl. Opt.*, *38*, 2346–2357, 1999a.

Müller, D., U. Wandinger, and A. Ansmann, Microphysical particle parameters from extinction and backscatter lidar data by inversion with regularization: Simulation, *Appl. Opt.*, *38*, 2358–2368, 1999b.

Pelon, J., P. H. Flamant, and M. Meisonnier, The French airborne backscatter lidar Leandre-1: Conception and operation, paper presented at 15th International Laser Radar Conference, Int. Coord., Gr. on Laser Atmos. Stud., Tomsk, 1990.

Pelon, J., C. Flamant, P. Chazette, J.-F. Leon, D. Tanre, M. Sicard, and S. K. Satheesh, Characterization of aerosol spatial distribution and optical properties over the Indian Ocean from airborne LIDAR and radiometry during INDOEX'99, *J. Geophys. Res.*, *107*(D19), 8029, doi:10.1029/2001JD000402, 2002.

Prospero, J. M., and T. N. Carlson, Vertical and areal distribution of Saharan dust over the western equatorial north Atlantic Ocean, *J. Geophys. Res.*, *77*, 5255–5265, 1972.

Remer, L. A., et al., Validation of MODIS aerosol retrieval over ocean, *Geophys. Res. Lett.*, *29*(12), 8008, doi:10.1029/2001GL013204, 2002.

Salomonson, V. V., W. L. Barnes, P. W. Maymon, H. E. Montgomery, and H. Ostrow, MODIS: Advanced facility instrument for studies of the Earth as a system, *IEEE Trans. Geosci. Remote Sens.*, *27*, 145–153, 1989.

Shettle, E. P., Optical and radiative properties of a desert aerosol model, in *Proceedings of the Symposium on Radiation in the Atmosphere*, edited by G. Fiocco, pp. 74–77, A. Deepak, Hampton, Va., 1984.

Sicard, M., P. Chazette, J. Pelon, J. G. Wong, and S.-C. Yoon, Variational method for the retrieval of the optical thickness and the backscatter coefficient from multiangle lidar profiles, *Appl. Opt.*, *41*, 493–502, 2002.

Tanré, D., M. Herman, and Y. J. Kaufman, Information on the aerosol size distribution contained in the solar reflected spectral radiances, *J. Geophys. Res.*, *101*, 19,043–19,060, 1996.

Tanré, D., Y. J. Kaufman, and S. Matoo, Remote sensing of aerosol properties over oceans using the MODIS/EOS spectral radiances, *J. Geophys. Res.*, *102*, 16,971–16,988, 1997.

Tanré D., et al., Measurement and modeling of the Saharan dust radiative impact: Overview of the Saharan Dust Experiment (SHADE), *J. Geophys. Res.*, *108*(D18), 8574, doi:10.1029/2002JD003273, 2003.

Wang, M., and H. R. Gordon, Estimating aerosol optical properties over the oceans with MISR: Some preliminary studies, *Appl. Opt.*, *33*, 4042–4057, 1994.

Welton, E. J., et al., Ground-based lidar measurements of aerosol during ACE-2: Instrument description, results, and comparisons with other ground-based and airborne measurements, *Tellus, Ser. B*, *52*, 636–651, 2000.

Whitby, K. Y., The physical characteristics of sulfur aerosols, *Atmos. Environ.*, *12*, 135–159, 1978.

Winker D., R. H. Couch, and M. P. McCormick, An overview of LITE: Nasa's lidar in-space technology experiment, *Proc. IEEE*, *84*, 164–180, 1996.

Winker, D., J. Pelon, and M. P. McCormick, The CALIPSO mission: Aerosol and cloud observations from space, in *21th International Lidar Radar Conference*, pp. 735–738, Int. Coord., Gr. on Laser Atmos. Stud., Québec, 8–10 July 2002.

Zuev, V. E., and I. E. Naats, Inverse Problems of Lidar Sensing of the Atmosphere, edited by Theodor Tamir, 260 pp., Springer-Verlag, New York, 1983.

B. Chatenet, Laboratoire Inter-Universitaire des Systèmes Atmosphériques, Centre National de la Recherche Scientifique, Université Paris 12, 61, avenue du Général de Gaulle, F-94010 Créteil, France. (chatenet@lisa.univ-paris12.fr)

J. M. Haywood, Met Office, Y46 Building, DERA, Fanborough, Hants GU14 0LX, UK. (jmhaywood@metoffice.com)

Y. Kaufman, Laboratory for Atmospheres, NASA Goddard Space Flight Center, Code 913, Greenbelt, MD 20771, USA. (kaufman@climate.gsfc.nasa.gov)

J.-F. Léon and D. Tanré, Laboratoire d'Optique Atmosphérique, Centre National de la Recherche Scientifique, Université de Lille 1, F-59655 Villeneuve-d'Ascq CEDEX, France. (leon@loa.univ-lille1.fr; tanre@loa.univ-lille1.fr)

J. Pelon, Service d'Aéronomie, Institut Pierre Simon Laplace, Centre National de la Recherche Scientifique, Université Pierre et Marie Curie, F-75252 Paris, France. (jacques.pelon@aero.jussieu.fr)